Inorganic Chemistry

Article

pubs.acs.org/IC

Versatile Reactivity of a Solvent-Coordinated Diiron(II) Compound: Synthesis and Dioxygen Reactivity of a Mixed-Valent $Fe^{II}Fe^{III}$ Species

Amit Majumdar,[†] Ulf-Peter Apfel,[†] Yunbo Jiang,[‡] Pierre Moënne-Loccoz,*[,‡] and Stephen J. Lippard*[,†]

[†]Department of Chemistry, Massachusetts Institute of Technology, Cambridge, Massachusetts 02139, United States

[‡]Division of Environmental and Biomolecular Systems, Institute of Environmental Health, Oregon Health and Science University, Portland, Oregon 97239, United States

Supporting Information

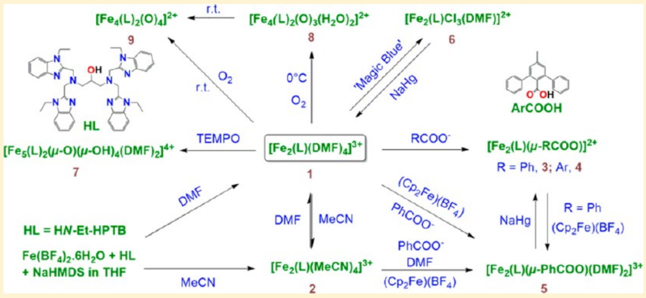

ABSTRACT: A new, DMF-coordinated, preorganized diiron compound $[Fe_2(N\text{-Et-HPTB})(DMF)_4](BF_4)_3$ (**1**) was synthesized, avoiding the formation of $[Fe(N\text{-Et-HPTB})](BF_4)_2$ (**10**) and $[Fe_2(N\text{-Et-HPTB})(\mu\text{-MeCONH})](BF_4)_2$ (**11**), where *N*-Et-HPTB is the anion of *N*,*N*,*N*′,*N*′-tetrakis[2-(1-ethylbenzimidazolyl)]-2-hydroxy-1,3-diaminopropane. Compound **1** is a versatile reactant from which nine new compounds have been generated. Transformations include solvent exchange to yield $[Fe_2(N\text{-Et-HPTB})(MeCN)_4](BF_4)_3$ (**2**), substitution to afford $[Fe_2(N\text{-Et-HPTB})(\mu\text{-RCOO})](BF_4)_2$ (**3**, R = Ph; **4**, RCOO = 4-methyl-2,6-diphenyl benzoate]), one-electron oxidation by $(Cp_2Fe)(BF_4)$ to yield a Robin−Day class II mixed-valent diiron(II,III) compound, $[Fe_2(N\text{-Et-HPTB})(\mu\text{-PhCOO})(DMF)_2](BF_4)_3$ (**5**), two-electron oxidation with tris(4-bromophenyl)aminium hexachloroantimonate to generate $[Fe_2(N\text{-Et-HPTB})Cl_3(DMF)](BF_4)_2$ (**6**), reaction with (2,2,6,6-tetramethylpiperidin-1-yl)oxyl to form $[Fe_5(N\text{-Et-HPTB})_2(\mu\text{-OH})_4(\mu\text{-O})(DMF)_2](BF_4)_4$ (**7**), and reaction with dioxygen to yield an unstable peroxo compound that decomposes at room temperature to generate $[Fe_4(N\text{-Et-HPTB})_2(\mu\text{-O})_3(H_2O)_2](BF_4)\cdot 8DMF$ (**8**) and $[Fe_4(N\text{-Et-HPTB})_2(\mu\text{-O})_4](BF_4)_2$ (**9**). Compound **5** loses its bridging benzoate ligand upon further oxidation to form $[Fe_2(N\text{-Et-HPTB})(OH)_2(DMF)_2](BF_4)_3$ (**12**). Reaction of the diiron(II,III) compound **5** with dioxygen was studied in detail by spectroscopic methods. All compounds (**1**−**12**) were characterized by single-crystal X-ray structure determinations. Selected compounds and reaction intermediates were further examined by a combination of elemental analysis, electronic absorption spectroscopy, Mössbauer spectroscopy, EPR spectroscopy, resonance Raman spectroscopy, and cyclic voltammetry.

INTRODUCTION

Bacterial multicomponent monoxygenases (BMMs) comprise a remarkable class of enzymes that catalyze the oxidation of aliphatic and aromatic hydrocarbons using naturally abundant dioxygen.[1−3] Soluble methane monooxygenase (sMMO),[1,4] the flagship of the BMM family, catalyzes the conversion of methane to methanol. Extensive structural studies revealed that the reduced hydroxylase component of sMMO ($sMMOH_{red}$) contains a diiron(II) core coordinated by two bridging and two terminal glutamate residues along with two imidazole groups disposed in a syn manner with respect to the iron−iron vector.[5−7] Spectroscopic and kinetic studies revealed fascinating redox reactions involved in the mechanistic pathway of dioxygen activation and substrate oxidation. This redox interplay involves oxygenated iron species, including diiron(III) peroxo and di(μ-oxo)diiron(IV) intermediates in the catalytic cycle of sMMO. A detailed account of this chemistry has recently appeared.[8] Descriptions of several model systems for the active site of $sMMOH_{red}$ and other diiron active sites as well as an account of their reactivity can be found elsewhere.[9−16]

Redox chemistry is a key feature in several steps of the catalytic cycle of sMMO,[8,17,18] which involves stepwise formation of the higher-valent diiron centers, substrate oxidation, and rereduction of the diiron(III) resting state to the intermediate mixed-valent $Fe^{II}Fe^{III}$ species and finally to an active diiron(II) species. Involvement of such intricate redox interplay is an incentive for bioinorganic chemists to test the potential of small-molecule model systems to mimic such redox reactions. Although a mixed-valent $Fe^{II}Fe^{III}$ state may not be catalytically relevant in most dioxygen-activating diiron enzymes,[4,8] *myo*-inositol oxygenase (MIOX)[19−22] is an exception. MIOX contains a nonheme diiron(II,III) cluster that catalyzes the unique, ring-cleaving, four-electron oxidation of *myo*-inositol to D-glucuronate. The enzyme MIOX is a key regulator of inositol levels, and the catalyzed reaction[19,21,23] is the first step in the glucuronate−xylulose pathway. One approach to provide insight into the chemical nature of such mixed-valent forms of the enzymes is to prepare and spectroscopically characterize diiron(II,III) complexes and to investigate their reactivity. Several such complexes having different ligand systems are known, and their spectroscopic

Received: July 29, 2013
Published: December 20, 2013

properties have been studied in detail.[24−31] However, few, if any, undergo reactions of relevance to dioxygen activation.

Although one can construct tailor-made dinucleating ligand systems that closely mimic the structures[32] of carboxylate-bridged diiron enzymes such as sMMOH$_{red}$, simple diiron compounds based on established dinucleating ligands are also valuable for testing the feasibility of stepwise redox reactions like those stated above. With the latter alternate route in mind, we prepared a diiron complex based on the H*N*-Et-HPTB ligand.[33] This ligand system has been successfully used in modeling chemistry.[31,34−37] Complexes of the type $[Fe^{II}_2(N\text{-Et-HPTB})(\mu\text{-}O_2X)]^{2+}$, where O_2X is an oxyanion bridge, have been reported recently in order to delineate factors affecting the carboxylate shift upon formation of diiron−dioxygen adducts.[38] Another recent report[39] includes photocatalytic activation of dioxygen by a diiron(II) complex upon irradiation of a system composed of the corresponding diiron(III) analogue based on H*N*-Et-HPTB, using a ruthenium(II)−polybipyridine-type complex as the photosensitizer and triethylamine as a sacrificial electron donor.

Here we report the synthesis and versatile reactivity of a *N*,*N*-dimethylformamide (DMF)-coordinated diiron(II) compound, **1** (Chart 1), that features no bridging carboxylate. Reactions of **1** include reversible solvent exchange, substitution, reversible one and two electron oxidations, reaction with a radical oxidant, and dioxygen chemistry leading to the isolation and characterization of 9 new compounds (Scheme 1) including a Robin-Day[40] Class II mixed valent diiron compound. Reaction of this diiron(II,III) species with dioxygen is described in detail for the first time. This report includes the synthesis, X-ray structure determinations, spectroscopic studies, cyclic voltammetry studies and reactivities of diiron complexes with or without bridging carboxylate ligands and some corresponding reactive intermediate species.

Chart 1. Abbreviations and Designations of Compounds[a]

$[Fe_2(N\text{-Et-HPTB})(DMF)_4](BF_4)_3$	**1**
$[Fe_2(N\text{-Et-HPTB})(MeCN)_4](BF_4)_3$	**2**
$[Fe_2(N\text{-Et-HPTB})(\mu\text{-PhCOO})](BF_4)_2$	**3**[34]
$[Fe_2(N\text{-Et-HPTB})(\mu\text{-ArCOO})](BF_4)_2$	**4**
$[Fe_2(N\text{-Et-HPTB})(\mu\text{-PhCOO})(DMF)_2](BF_4)_3$	**5**
$[Fe_2(N\text{-Et-HPTB})Cl_3(DMF)](BF_4)_2$	**6**
$[Fe_5(N\text{-Et-HPTB})_2(\mu\text{-OH})_4(\mu\text{-O})(DMF)_2](BF_4)_4$	**7**
$[Fe_4(N\text{-Et-HPTB})_2(\mu\text{-O})_3(H_2O)_2](BF_4)_2$	**8**
$[Fe_4(N\text{-Et-HPTB})_2(\mu\text{-O})_4](BF_4)_2$	**9**
$[Fe(N\text{-Et-HPTB})](BF_4)_2$	**10**
$[Fe_2(N\text{-Et-HPTB})(\mu\text{-MeCONH})](BF_4)_2$	**11**
$[Fe_2(N\text{-Et-HPTB})(OH)_2(DMF)_2](BF_4)_3$	**12**

[a] H*N*-Et-HPTB, (*N*,*N*,*N*′,*N*′-tetrakis[2-(l-ethylbenzimidazolyl)]-2-hydroxy-1,3-diaminopropane; ArCOOH, 4-methyl-2,6-diphenylbenzoic acid; "magic blue", tris(4-bromophenyl)aminium hexachloroantimonate; TEMPO, (2,2,6,6-tetramethylpiperidin-1-yl)oxyl; HBPMP, 2,6-bis[[bis(2-pyridylmethyl)amino]methyl]-4-methylphenol; OPr, propionate; HXTA, *N*,*N*′-(2-hydroxy-5-methyl-1,3-xylylene)bis[*N*-(carboxymethyl)glycine]; Hbimp, 2,6-bis[[bis[(1-methylimidazol-2-yl)methyl]amino]methylphenol; Me_3tacn, 1,4,7-trimethyl-1,4,7-triazacyclononane; HB(Pz′)$_3$, hydrotris(3,5-diisopropylpyrazolyl) borate; HPh-bimp, 2,6-bis[[bis(*N*-methyl-4,5-diphenylimidazole-2-yl)methyl]-aminomethyl]-4-methylphenol.

■ EXPERIMENTAL SECTION

Preparation of Compounds. All reactions and manipulations were performed under a pure dinitrogen atmosphere using either Schlenk techniques or an inert-atmosphere box. Solvents were passed through a solvent purification system prior to use. In the preparations that follow, reactants were used as suspensions or solutions in solvents of specified volume, filtrations were performed through Celite, solvent removal steps were carried out in vacuo, and products were washed with ether and dried. H*N*-Et-HPTB was synthesized according to a literature procedure.[33] $Fe(BF_4)_2\cdot 6H_2O$, NaHMDS, tris(4-bromophenyl)aminium hexachloroantimonate ("magic blue"), sodium benzoate, and anhydrous DMF were obtained from commercial sources and used without further purification. Yields are reported for recrystallized compounds. The identities of all 12 compounds in Chart 1 were confirmed by single-crystal X-ray structure determinations. Compound **3** was previously reported[34] without the DMF molecules in the lattice. A compound analogous to **5** was recently reported.[31] Selected compounds were further characterized by elemental analysis and studied by electronic absorption, electron paramagnetic resonance (EPR), and Mössbauer spectroscopy. All iron(II) compounds are extremely air-sensitive and must be handled accordingly.

[Fe$_2$(*N*-Et-HPTB)(DMF)$_4$](BF$_4$)$_3$ (1). To a suspension of H*N*-Et-HPTB (0.2 mmol, 144 mg) in 2 mL of tetrahydrofuran (THF) was added NaHMDS (0.2 mmol, 37 mg) in 2 mL of THF with stirring. After 1 min, $Fe(BF_4)_2\cdot 6H_2O$ (0.4 mmol, 135 mg) in 2 mL of THF was added, and the resultant slurry was stirred for 2 h. This slurry was filtered and the solid collected, washed with cold THF, and dried. The solid was dissolved in DMF and filtered, and the filtrate was diffused overnight with Et_2O at −45 °C with 1 day of additional standing at room temperature (RT) to yield a pale-yellow crystalline solid. This solid was recrystallized twice in the same manner to generate the product as colorless crystals (167 mg, 60%). Anal. Calcd for $C_{55}H_{77}B_3F_{12}Fe_2N_{14}O_5$ (**1**): C, 47.67; H, 5.60; N, 14.14. Found: C, 47.52; H, 5.32; N, 13.89.

[Fe$_2$(*N*-Et-HPTB)(MeCN)$_4$](BF$_4$)$_3$ (2). To a suspension of H*N*-Et-HPTB (0.2 mmol, 144 mg) in 2 mL of THF was added NaHMDS (0.2 mmol, 37 mg) in 2 mL of THF with stirring. After 1 min, $Fe(BF_4)_2\cdot 6H_2O$ (0.4 mmol, 135 mg) in 2 mL of THF was added, and the resultant slurry was stirred for 2 h. By following the workup procedure for **1** but using MeCN instead of DMF, the product was obtained as a colorless crystalline solid (160 mg, 60%).

Alternatively, the compound could be prepared by dissolving **1** in MeCN followed by overnight diffusion of Et_2O at −45 °C and 1 day of additional standing at RT, affording the product as a colorless crystalline solid in similar yield.

Despite repeated attempts, it was not possible to obtain satisfactory elemental analyses.

[Fe$_2$(*N*-Et-HPTB)(*μ*-PhCOO)](BF$_4$)$_2$ (3). To a solution of **1** (0.05 mmol, 69 mg) in 2 mL of MeCN was added PhCOONa (0.05 mmol, 7 mg) in 2 mL of MeCN, and the mixture was stirred for 6 h. The yellowish solution was evaporated to dryness. The residue was extracted with 1 mL of DMF and filtered, and the filtrate was diffused overnight with Et_2O at −45 °C and allowed to stand for 1 day at RT to afford the product as a light-yellow crystalline solid (42 mg, 66%).

Alternatively, this compound can be prepared directly from H*N*-Et-HPTB, $Fe(BF_4)_2\cdot 6H_2O$, PhCOOH, and Et_3N in methanol by following a method reported earlier.[34] The product was recrystallized by Et_2O diffusion into a DMF solution as light-yellow needles in 78% yield.

[Fe$_2$(*N*-Et-HPTB)(*μ*-ArCOO)](BF$_4$)$_2$ (4). To a mixture of H*N*-Et-HPTB (0.2 mmol, 144 mg) and 4-methyl-2,6-diphenylbenzoic acid (0.2 mmol, 58 mg) suspended in 4 mL of THF was added NaHMDS (0.4 mmol, 74 mg) in 2 mL of THF with stirring. After 1 min, $Fe(BF_4)_2\cdot 6H_2O$ (0.4 mmol, 135 mg) in 2 mL of MeCN was added, Scheme 1. Schematic Depiction of the Syntheses of Complexes 1−9 and 12 (Chart 1)

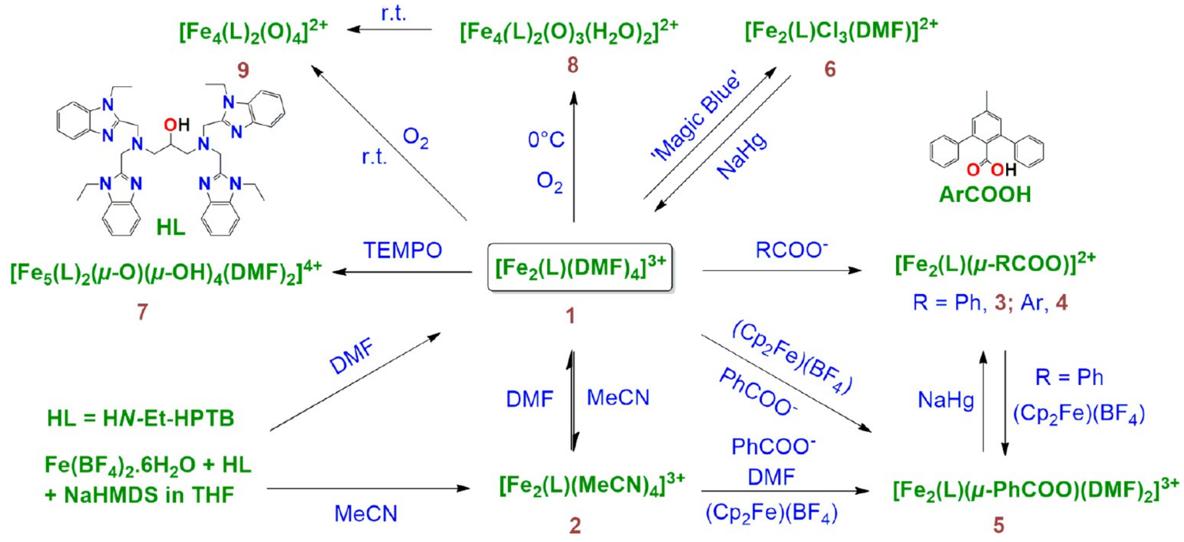

causing a transient violet color, which eventually afforded a colorless solution and subsequently a nearly colorless slurry upon stirring for 6 h. By following the workup procedure for **3**, the product was obtained as a colorless crystalline solid (235 mg, 81%). Anal. Calcd for $C_{69}H_{78}B_2F_8Fe_2N_{12}O_5$ (**4**·2DMF): C, 57.52; H, 5.46; N, 11.67. Found: C, 57.18; H, 5.16; N, 11.55.

Fe_2(*N*-Et-HPTB)(μ-PhCOO)($DMF)_2$]($BF_4)_3$ (5). To a solution of **1** (0.05 mmol, 69 mg) in 2 mL of MeCN was added, with stirring, a suspension of PhCOONa (0.05 mmol, 7 mg) in 2 mL of MeCN followed by addition of a solution of $(Cp_2Fe)(BF_4)$ (0.05 mmol, 14 mg) in 2 mL of MeCN. The mixture was stirred for 6 h. The greenish-brown solution was evaporated to dryness, and the residue thus obtained was thoroughly washed with THF to afford a brown solid. By following the workup procedure for **3**, the product was obtained as a brown crystalline solid (30 mg, 40%).

Alternatively, this compound can be prepared from **3**. A solution of $(Cp_2Fe)(BF_4)$ (0.05 mmol, 14 mg) in 2 mL of MeCN was added to a solution of **3** (0.05 mmol, 64 mg) in MeCN and stirred for 4 h. By following the workup procedure for **3**, the product was obtained as dark-red-brown crystals (50 mg, 63%). Anal. Calcd for $C_{62}H_{84}B_3F_{12}Fe_2N_{14}O_8$ (**5**·2DMF·H_2O): C, 48.81; H, 5.55; N, 12.85. Found: C, 48.77; H, 5.13; N, 12.79.

[Fe_2(*N*-Et-HPTB)Cl_3(DMF)]($BF_4)_2$ (6). To a solution of **1** (0.05 mmol, 69 mg) in 2 mL of MeCN was added a solution of tris(4-bromophenyl)aminium hexachloroantimonate (0.06 mmol, 49 mg) in 2 mL of MeCN. The mixture was stirred for 6 h. The orange solution was evaporated to dryness. By following the workup procedure for **3**, the product was obtained as an orange crystalline solid (40 mg, 65%). This compound gave a slightly low carbon analysis. Anal. Calcd for $C_{46}H_{56}B_2Cl_3F_8Fe_2N_{11}O_2$ (**6**): C, 46.52; H, 4.76; N, 12.98. Found: C, 45.87; H, 4.78; N, 12.91.

[Fe_5(*N*-Et-HPTB)$_2$(μ-OH)$_4$(μ-O)(DMF)$_2$]($BF_4)_4$ (7). To a solution of **1** (0.05 mmol, 69 mg) in 1 mL of DMF was added a solution of TEMPO (0.1 mmol, 16 mg) in 1 mL of DMF, and the mixture was stirred for 12 h. This solution was diffused for 2 days with Et_2O at −45 °C with 1 day of additional standing at RT to obtain the product as light-red crystals. This compound was characterized by an X-ray structure determination.

[Fe_4(*N*-Et-HPTB)$_2$(μ-O)$_4$]($BF_4)_2$ (9). Dioxygen was bubbled into a solution of **1** (0.05 mmol, 69 mg) in 1 mL of DMF for 1 min. This solution was diffused with Et_2O at RT for 2 days to obtain the product as red-brown crystals (34 mg, 66%).

When dioxygen was bubbled into a solution of identical composition that had been precooled to 0 °C followed by ether diffusion at 0 °C for 2 days and subsequent standing at RT for 1 day, the product obtained was a mixture of **9** (major product) and [Fe_4(*N*-Et-HPTB)$_2$(μ-O)$_3$($H_2O)_2$](BF_4) (**8**; minor product). The latter was identified by an X-ray structure determination only and was never obtained in appreciable quantities as a pure compound.

[Fe(*N*-Et-HPTB)]($BF_4)_2$ (10) and [Fe_2(*N*-Et-HPTB)(μ-MeCONH)]($BF_4)_2$ (11). To a suspension of H*N*-Et-HPTB (0.5 mmol, 361 mg) in 2 mL of THF was added NaHMDS (0.51 mmol, 94 mg) in 2 mL of THF. After 1 min, $Fe(BF_4)_2$·6H_2O (1 mmol, 336 mg) in 4 mL of MeCN was added, and the mixture was stirred for 4 h. The reaction mixture was then evaporated to dryness. The residue obtained was insoluble in THF, MeCN, and dichloromethane (DCM). It was dissolved in DMF and filtered, and the filtrate was diffused overnight with Et_2O at −45 °C with 1 day of additional standing at RT to afford a mixture of **1**, **10**, and **11**. The latter two compounds were identified by X-ray structure determinations only. No attempts were made to prepare them in pure form.

[Fe_2(*N*-Et-HPTB)(OH)$_2$(DMF)$_2$]($BF_4)_3$ (12). To a solution of **5** (0.05 mmol, 79 mg) in 2 mL of MeCN was added, with stirring, a solution of $(Cp_2Fe)(BF_4)$ (0.06 mmol, 17 mg) in 2 mL of MeCN. The mixture was stirred for 24 h. By following the workup procedure for **5**, the product was obtained as a brown crystalline solid (26 mg).

Alternatively, this compound can be prepared from **3**. A solution of $(Cp_2Fe)(BF_4)$ (0.12 mmol, 33 mg) in 2 mL of MeCN was added to a solution of **3** (0.05 mmol, 4 mg) in MeCN and stirred for 24 h. By following the workup procedure for **5**, the product was obtained as a brown crystalline solid (24 mg).

Irrespective of the procedure, **12** was never obtained as a pure material in bulk quantities and was contaminated with **5** as identified by unit cell determinations, solution stability comparisons in the presence of dioxygen, and cyclic voltammetry. Compound **12** was characterized only by a single-crystal X-ray structure determination.

General Physical Methods. Electronic absorption spectra were recorded on either a Cary 1 or a Cary 50 spectrophotometer using 6Q Spectrosil quartz cuvettes (Starna) with a 1 cm path length. X-band EPR spectra were recorded at 77 K on a Bruker EMX spectrometer. Electrochemical measurements were performed with 1 mM solutions of samples in DMF using a VersaSTAT3 Princeton Applied Research potentiostat running the *V3-Studio* electrochemical analysis software. A three-electrode setup was employed comprising a platinum working electrode, a platinum wire auxiliary electrode, and a silver rod as the pseudo reference electrode. Tetra-*n*-butylammonium hexafluorophosphate (0.1 M) was used as the supporting electrolyte. Electrochemical potentials are referenced internally to the ferrocene/ferrocenium couple at 0.00 V.

^{57}Fe Mössbauer Spectroscopy. Mössbauer spectra were recorded on an MSI spectrometer (WEB Research Co.) with a ^{57}Co source in a rhodium matrix maintained at RT. Solid samples were prepared by a suspension of the complex (40−50 mg) in Apiezon M grease and placed in a nylon sample holder. All samples contained

Table 1. X-ray Crystallographic Data for Compounds 1−6 (Chart 1) at 100 K[a]

	1	2·2MeCN	3·2DMF	4·2DMF	5·3DMF	2(6)·Et_2O
formula	$C_{55}H_{77}B_3F_{12}Fe_2N_{14}O_5$	$C_{55}H_{67}B_3F_{12}Fe_2N_{16}O$	$C_{56}H_{68}B_2F_8Fe_2N_{12}O_5$	$C_{69}H_{78}B_2F_8Fe_2N_{12}O_5$	$C_{65}H_{89}B_3F_{12}Fe_2N_{15}O_8$	$C_{96}H_{122}B_4Cl_6F_{16}Fe_4N_{22}O_5$
fw	1386.44	1340.38	1274.54	1440.75	1580.64	2447.50
cryst syst	triclinic	triclinic	triclinic	triclinic	triclinic	monoclinic
space group	$P\bar{1}$	$P\bar{1}$	$P\bar{1}$	$P\bar{1}$	$P\bar{1}$	$P2_1/c$
a, Å	12.629(8)	14.656(6)	13.016(1)	12.150(2)	19.182(9)	19.606(8)
b, Å	15.415(10)	16.035(6)	13.827(2)	16.280(2)	19.943(9)	21.522(9)
c, Å	17.705(1)	16.885(6)	18.859(2)	17.653(2)	20.448(9)	17.649(7)
α, deg	78.326(1)	112.807(1)	72.271(2)	98.098(2)	99.085(1)	
β, deg	86.512(1)	94.447(1)	80.965(2)	95.663(2)	105.025(1)	114.826(1)
γ, deg	68.977(1)	110.424(1)	67.018(2)	101.203(2)	97.781(1)	
V, Å^3	3150.5(4)	3321.4(2)	2973.4(6)	3362.3(8)	7331.1(6)	6759.2(5)
Z	2	2	2	2	4	2
ρ_{calcd}, g cm^{-3}	1.462	1.340	1.424	1.423	1.432	1.203
μ, mm^{-1}	0.555	0.520	0.571	0.514	0.490	0.611
θ range, deg	1.67−25.69	1.51−25.69	1.66−26.01	1.60−25.73	1.63−25.62	1.14−25.74
completeness to θ, %	99.8	99.8	99.1	99.0	99.8	99.9
no. of reflns collected	51577	55393	44835	53875	119525	108108
no. of indep reflns	11969	12625	11587	12706	27612	12909
R(int)	0.0251	0.0250	0.0470	0.0297	0.0298	0.0405
no. of restraints[d]	7	0	11	0	56	16
no. of param	844	830	835	892	1949	771
max, min transmn	0.9570, 0.8602	0.9498, 0.8596	0.9451, 0.7954	0.9797, 0.8865	0.9619, 0.8512	0.9760, 0.7921
R1[b] (wR2)[c] [$I > 2\sigma(I)$]	0.0513 (0.1236)	0.0348 (0.0927)	0.0728 (0.1650)	0.0381 (0.1016)	0.0577 (0.1545)	0.0595 (0.1899)
R1[b] (wR2)[c]	0.0597 (0.1301)	0.0411 (0.0958)	0.1290 (0.2235)	0.0483 (0.1090)	0.0733 (0.1689)	0.0708 (0.1999)
GOF(F^2)[d]	1.028	1.056	1.013	1.044	1.055	1.065
max, min peaks,[e] e Å^{-3}	1.924, −1.825	0.918, −0.726	1.241, −0.800	0.862, −0.488	1.919, −2.161	2.330, −0.870

[a] Mo Kα radiation (λ = 0.71073 Å). [b] $R1 = \sum||F_o| - |F_c|| / \sum|F_o|$. [c] $wR2 = \{\sum[w(F_o^2 - F_c^2)^2] / \sum[w(F_o^2)^2]\}^{1/2}$. [c] $GOF = \{\sum[w(F_o^2 - F_c^2)^2]/(n - p)\}^{1/2}$, where n is the number of data and p is the number of refined parameters. [d] **1**, disordered DMF; **3**, disordered BF_4^- (2), *N*-Et group (3), DMF (1), and phenyl ring (1); **5**, disordered BF_4^- (1), DMF (1), *N*-Et group (1); **6**, disordered DMF (2), *N*-Et group (1), Et_2O (1). [e] **1**, electron density near one BF_4^-, disorder modeling was not reasonable; **3**, electron density near one of the phenyl rings, disorder modeling was not reasonable; **5**, near one of the disorder-modeled BF_4^-; **6**, near disorder-modeled diethyl ether, reasonable modeling was not found.

natural abundance iron and were measured over the course of 1−2 days. Data were acquired at 77 K, and isomer shift (δ) values are reported with respect to an α-iron foil that was used for velocity calibration at RT. Spectra were fit to Lorentzian line shapes using the *WMOSS* plot and fit program.

Resonance Raman (RR) Spectroscopy. RR samples were prepared by injecting 6 mM DMF solutions of compound **5** in NMR tubes filled with $^{16}O_2$ or $^{18}O_2$ gas. The reaction was allowed to proceed for 6 min at RT before the samples were frozen in liquid nitrogen. RR spectra were collected on a McPherson 2061/207 spectrometer equipped with a Princeton Instrument liquid-nitrogen-cooled CCD detector (LN-1100 PB). The 647 nm excitation was provided by a Coherent Innova 302C krypton ion laser, and a matching long-wave pass filter (RazorEdge filter, Semrock) was used to attenuate the Rayleigh scattering. Frequencies were calibrated relative to several frequency standards and are accurate to ±1 cm^{-1}. The samples were placed in a copper coldfinger cooled with liquid nitrogen to maintain the sample temperature at ~110 K during data acquisition. Individual spectra obtained at different laser power and with or without sample spinning were compared to confirm the integrity of the samples during data acquisition.

X-ray Structure Determinations. The structures of the compounds shown in Chart 1 were determined. Diffraction-quality crystals were obtained by ether diffusion into MeCN or DMF solutions as described in the respective syntheses. Single crystals were mounted in Paratone oil using 30-μm-aperture MiTeGen MicroMounts (Ithaca, NY) and frozen under a 100 K KRYO-FLEX nitrogen cold stream. Data were collected on a Bruker SMART APEX CCD X-ray diffractometer with Mo Kα radiation (λ = 0.71073 Å) controlled by the *APEX2* (version 2010.1-2) software package. Raw data were integrated and corrected for Lorentz and polarization effects using the Bruker *APEX II* program suite.[41] Absorption corrections were performed using *SADABS*. Space groups were assigned by analysis of the metric symmetry and systematic absences (determined by *XPREP*) and were further checked by *PLATON*[42,43] for additional symmetry. Structures were solved by direct methods and refined against all data in the reported 2θ ranges by full-matrix least squares on F^2 with the *SHELXL* program suite[44] using the *OLEX2* interface.[45] Hydrogen atoms at idealized positions were included in final refinements. The *OLEX2* interface was used for structure visualization and drawing of the ORTEP plots.[46,47] Crystallographic data and final agreement factors for complexes **1**−**12** are given in Tables 1 and 2 along with explanations for restraints used and positions of residual electron densities. Most of the compounds contain disordered anions, solvents, and/or parts of a ligand and are mentioned for individual compounds in the footnotes of Tables 1 and 2. These features were taken care of by disorder modeling using free variables (PART instructions) along with appropriate restraints (SADI and EADP). Compound **5** contains two independent molecules in its asymmetric unit ($P\bar{1}$; Z = 4). These two independent units display different Fe−O bond distances. X-ray structures of **2**, **6**, **8**, **9**, and **12** contained several severely disordered solvent molecules. Their contributions to the structure factors were taken into account either by applying the *MASK* procedure in the *OLEX2* program package (**2**, **8**, **9**, and **12**) or by using the *SQUEEZE* procedure in *PLATON* (**6**). Solvent-accessible voids and total electron counts per cell for **2**, **6**, **8**, **9**, and **12** are 736.6

Table 2. X-ray Crystallographic Data for Compounds 7−12 (Chart 1) at 100 K[a]

	73DMF·E·t$_2$O	**8**·2DMF	**9**·2DMF	**10**·4MeCN	**11**·DMF	**12**·2DMF
formula	$C_{105}H_{150}B_4F_{16}Fe_5N_{25}O_{13}$	$C_{92}H_{116}B_2F_8Fe_4N_{22}O_9$	$C_{92}H_{112}B_2F_8Fe_4N_{22}O_8$	$C_{51}H_{62}B_2F_8FeN_{14}O$	$C_{48}H_{60}B_2F_8Fe_2N_{12}O_3$	$C_{55}H_{78}B_3F_{12}Fe_2N_{14}O_7$
fw	2596.99	2071.09	2051.06	1116.62	1138.40	1419.44
cryst syst	triclinic	triclinic	triclinic	orthorhombic	monoclinic	triclinic
space group	$P\bar{1}$	$P\bar{1}$	$P\bar{1}$	$Pbcn$	$P2_1/n$	$P\bar{1}$
a, Å	17.548(2)	15.092(2)	17.282(1)	23.978(2)	13.879(1)	12.821(4)
b, Å	18.524(2)	17.612(3)	17.599(1)	11.555(8)	23.342(2)	17.528(6)
c, Å	20.896(2)	27.955(4)	23.455(3)	19.580(1)	15.968(1)	17.703(6)
α, deg	78.952(2)	85.993(3)	100.636(2)			73.288(1)
β, deg	71.109(2)	80.605(2)	95.959(2)		97.122(2)	76.650(1)
γ, deg	69.479(2)	64.731(2)	116.188(1)			79.532(1)
V, Å^3	5995.2(1)	6629.1(2)	6151.0(1)	5425.0(6)	5133.0(8)	3678.9(2)
Z	2	2	2	4	4	2
ρ_{calcd}, g cm^{-3}	1.439	1.257	1.107	1.367	1.473	1.281
μ, mm^{-1}	0.684	0.506	0.527	0.357	0.649	0.478
θ range, deg	1.63−25.76	1.48−25.80	1.61−24.75	1.70−25.71	1.55−25.69	1.49−25.70
completeness to θ, %	99.1	99.0	98.6	100.0	100.0	99.8
no. of reflns collected	95976	25264	92034	84107	83460	58867
no. of indep reflns	22796	107121	20801	5165	9751	13988
R(int)	0.0585	0.0630	0.0457	0.0422	0.0469	0.0365
no. of restraints[d]	16	6	3	3	46	17
no. of param	1509	1269	1161	360	668	791
max, min transmn	0.9731, 0.8210	0.9899, 0.8629	0.9691, 0.8169	0.9858, 0.9385	0.9745, 0.9262	0.9811, 0.9104
R1[b] (wR2)[c] [$I > 2\sigma(I)$]	0.0841 (0.2271)	0.0809 (0.2559)	0.0762 (0.2433)	0.0652 (0.1622)	0.0912 (0.2200)	0.0848 (0.2554)
R1[b] (wR2)[c]	0.1140 (0.2484)	0.1157(0.2789)	0.0959 (0.2587)	0.0776 (0.1737)	0.1089 (0.2335)	0.1110 (0.2771)
GOF(F^2)[d]	1.073	1.116	1.096	1.057	1.051	1.143
max, min peaks,[e] e Å^{-3}	1.821, −1.137	1.096, −0.675	1.118, −1.136	1.467, −0.951	1.232, −1.101	1.473, −1.418

[a] Mo Kα radiation (λ = 0.71073 Å). [b] $R1 = \sum||F_o| - |F_c||/\sum|F_o|$. [c] $wR2 = \{\sum[w(F_o^2 - F_c^2)^2]/\sum[w(F_o^2)^2]\}^{1/2}$. [c] $GOF = \{\sum[w(F_o^2 - F_c^2)^2]/(n - p)\}^{1/2}$, where n is the number of data and p is the number of refined parameters. [d] **7**, disordered DMF (2), diethyl ether (1); **8**, disordered DMF (2), *N*-Et group (2); **9**, disordered DMF(1), *N*-Et group (1); **10**, MeCN (3); **11**, disordered DMF (1), BF_4^- (2), *N*-Et (2), *N*-CH (4); **12**, disordered DMF (1), perchlorate (3). [e] **7**, near one BF_4^-, disorder modeling was not reasonable; **8**, near iron; **9**, near BF_4^-, disorder modeling was not helpful; **10**, near the alkoxide group, not taken into account; **11**, near severely disordered benzimidazole; **12**, near hydroxide groups, no meaningful disorder modeling found; **13**, near one of the perchlorates, disorder modeling was not helpful.

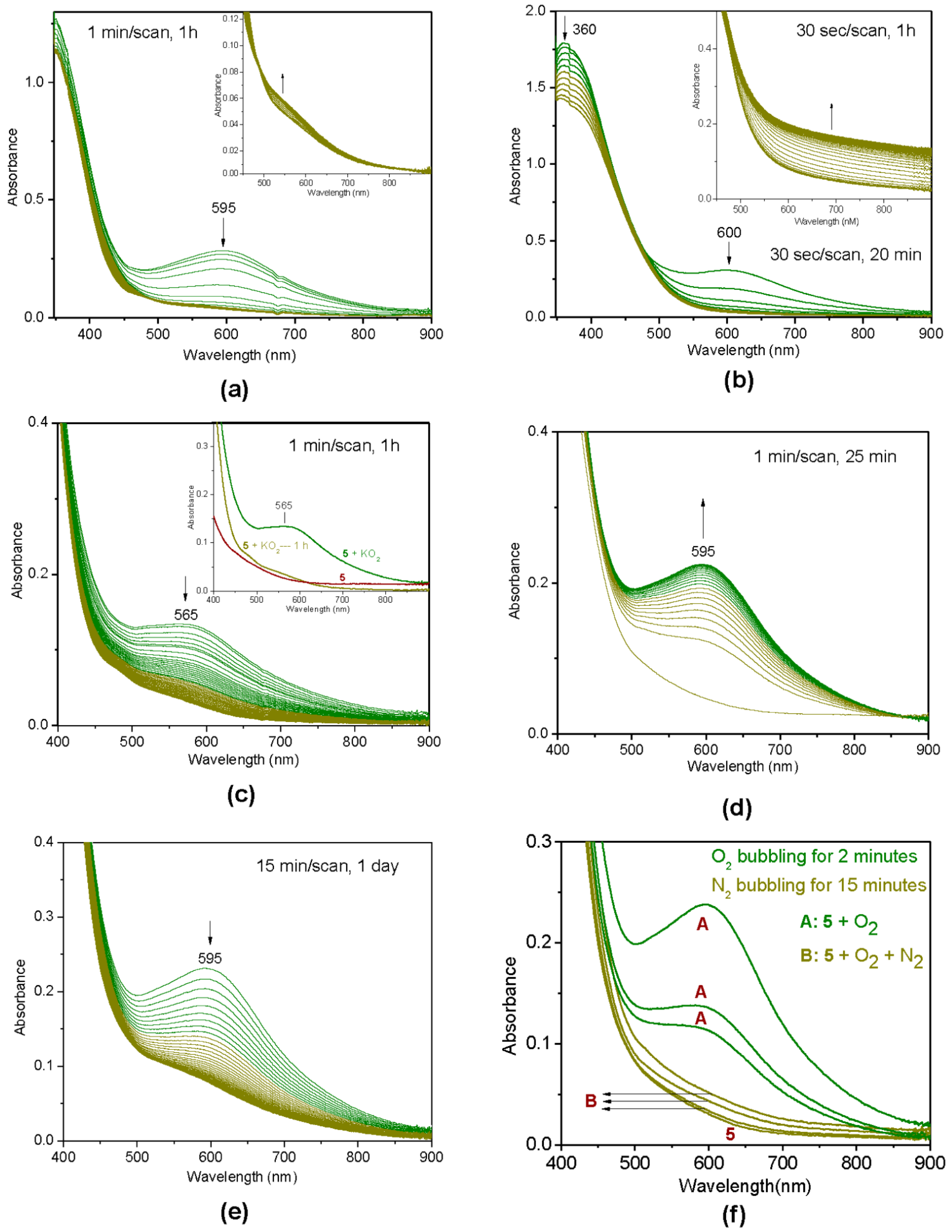

Figure 1. Electronic absorption spectroscopic monitoring at RT of (a) decomposition of in situ generated peroxo species ($1 + O_2$) in DMF. [**1**] = 0.0002 M. Inset: magnified view of the second stage of decomposition. (b) Decomposition of in situ generated peroxo species ($1 + O_2$) in CH_2Cl_2. [**1**] = 0.0002 M. Inset: second stage of decomposition measured separately. (c) Decomposition of the oxidized species formed by reaction of **5** ([**5**] = 0.0002 M) with KO_2 (0.0005 M) in the presence of 18-crown-6 (0.0005 M) in DMF. Inset: absorption spectra for selected stages of the experiment. (d) Reaction of **5** ([**5**] = 0.0002 M) with dioxygen (5 s of bubbling), forming a green solution in DMF. (e) Decomposition of the green species upon standing at RT. (f) Demonstration of quasi-reversibility for the formation of the green species by reaction of compound **5** with dioxygen.

Å^3, 115.7; 657 Å^3, 224; 2485.6 Å^3, 183.8; 1888.6 Å^3, 279.2; and 541.0 Å^3, 86.9, respectively. Refinement details and explanations (wherever necessary) are included in the individual CIFs.

■ RESULTS AND DISCUSSION

Synthesis. Compound **1** was prepared by addition of an iron(II) salt to a solution of deprotonated H*N*-Et-HPTB in THF. The choice of solvent is of utmost importance because the same reaction in MeCN or in a 1:1 mixture of THF and MeCN yields a mixture of compounds **1**, Fe(*N*-Et-HPTB)]$(BF_4)_2$ (**10**), and [Fe_2(*N*-Et-HPTB)(μ-MeCONH)]$(BF_4)_2$ (**11**). The bridging acetamide in **11** was probably generated by base-catalyzed (NaHMDS) partial hydrolysis of MeCN. Hydrolysis of MeCN in the presence of iron compounds is precedented.[48] This problem was avoided by use of THF as the sole solvent and filtration followed by thorough washing with THF to obtain a pale greenish-yellow solid prior to use of MeCN or DMF as the solvent for crystallization to obtain **2** or **1**, respectively, as colorless crystals. To the best of our knowledge, **1** and **2** do not have any precedent in the literature except for a diiron(III) compound, reported only recently[39] while this manuscript was in preparation. Compound **1** offers a rich chemistry involving solvent exchange, substitution, dioxygen reactivity, and controlled redox reactions, leading in this study to the isolation and X-ray structural characterization of nine compounds (**2**–**9** and **12**), as presented in Scheme 1. Electronic absorption spectroscopic signatures of selected compounds are provided in the Supporting Information (Figure S1). The coordinated DMF molecules in **1** are easily displaced by MeCN to yield compound **2** by simple dissolution of **1** in MeCN and diffusion of Et_2O into the resulting solution. Alternatively, **2** can be directly prepared as described in the Experimental Section.

Compound **1** can be treated as a basic framework for preparing carboxylate-bridged diiron complexes, as shown by the syntheses of **3** with a bridging benzoate and **4** with a sterically demanding *m*-terphenyl carboxylate. The most important aspect of the reactivity of **1** is the possibility of one- and two-electron oxidations. One-electron oxidation of **1** with 1 equiv of $(Cp_2Fe)(BF_4)$, followed by immediate addition of sodium benzoate, yielded the class II mixed-valent ($Fe^{II}Fe^{III}$) compound **5**. Alternatively, **5** can be prepared by reaction of **3**[34] and 1 equiv of $Cp_2Fe(BF_4)$. Use of 2 equiv of $Cp_2Fe(BF_4)$ leads to loss of the carboxylate bridge, as shown by the isolation of the diiron(III) compound **12** in low yield. The hydroxo groups in **12** may have originated either from water carried over from $Fe(BF_4)_2{\cdot}6H_2O$ used to prepare **1** and **3**[34] or from adventitious moisture in otherwise dry solvents. Compound **5** can be converted back to **3**[34] by treatment with 1 equiv of NaHg, as confirmed by X-ray structural analysis. On the other hand, reaction of **1** with 1 equiv of "magic blue" (Chart 1) yielded an orange diiron(III) compound (**6**) in 65% yield. In this reaction, both tris(4-bromophenyl)aminium cation ($E°_{red}$ = 0.70 V vs ferrocene)[49] and hexachloroantimonate anion may each have acted as one-electron oxidants accompanied by chloride abstraction by the resulting iron(III) centers. Another possibility is that the hexachloroantimonate anion serves as two-electron oxidant, with concomitant chloride abstraction by the iron(III) centers. These modes of reaction by $SbCl_6^-$ coupled with subsequent halogenation in the case of organometallic complexes are well documented.[50] Interestingly, reduction of **6** using NaHg gives back compound **1**, as confirmed by a unit cell determination of a single crystal grown from Et_2O diffusion into a DMF solution of the isolated colorless product. Formation of **11** is frequently also observed along with **1**. This reaction can be visually monitored by the gradual bleaching of the dark orange-red color of **6** to yield a nearly colorless solution upon addition of NaHg in portions until a total of 2.5 equiv is used. Reaction of TEMPO with **1** was not well behaved, and only trace amounts of a red crystalline product (**7**) were isolated at an unconvincing stoichiometry of reactants. This chemistry was not further pursued.

Dioxygen Reactivity of 1. Compound **1** is highly reactive toward dioxygen, as monitored by absorption spectroscopy in both coordinating (DMF, Figure 1a) and noncoordinating (DCM, Figure 1b) solvents. Upon bubbling dioxygen through a colorless solution of **1** in DMF, the solution immediately developed a dark-green color corresponding to a visible band at 595 nm (600 nm in DCM solution), suggesting the formation of a peroxo species. Appearance of a visible band at 588 nm was reported upon exposure of a DCM solution of **3**[34] to dioxygen at −60 °C, whereas a visible band at 570 nm was observed upon similar conditions in the case of a diferrous propionate analogue of **3**.[34] These observations suggest the presence of a spectral band arising from a peroxo-to-iron(III) charge-transfer transition.[34] The difference between the absorption maxima (600 nm in the case of **1** + O_2, compared with 588 and 570 nm) in the same solvent (DCM) and same ligand system (H*N*-Et-HPTB) can be attributed to the absence of a bridging carboxylate in **1**. Dioxygen presumably binds to the open coordination sites of **1** and is reduced to the peroxide oxidation state by the iron centers. At RT, the green color of the solution slowly changes to light brown within 1 h and then to red-brown over the course of 8 h. Similar observations were noted upon changing the solvent from DMF to DCM, although, as expected, the dark-green peroxo compound seemed to be less stable in noncoordinating and less polar DCM compared to coordinating and more polar DMF. This result is consistent with previous reports that highly polar solvents such as DMF or DMSO stabilize dioxygen adducts.[34] Two compounds have been isolated and characterized (**8** and **9**) that may correspond to those responsible for the color changes (light brown, **8**, $2Fe^{II}$, $2Fe^{III}$; red-brown, **9**, all Fe^{III}) observed during the UV–vis spectroscopic study (Figure 1). Formation of such (μ-oxo)polyiron(III) species upon decomposition of related peroxodiiron(III) compounds has been previously proposed.[37] A recent report describes the dioxygen reactivity of several complexes of the type $[Fe^{II}_2(N\text{-Et-HPTB})(\mu\text{-}O_2X)]^{2+}$ (O_2X is an oxyanion bridge).[38] These diiron(II) complexes react with dioxygen in DCM at −90 °C to form triply bridged (μ-η^1:η^1-peroxo)diiron(III) species. With one exception (O_2X = O_2AsMe_2), all of these triply bridged intermediates (λ_{max} = 630–710 nm) convert irreversibly to doubly bridged species (λ_{max} = 580–620 nm) by expulsion of the bridging O_2X unit before decaying to yellow final products. Compound **1** does not have any bridging unit, and it generates an absorption maximum at 595 nm in a DMF (600 nm in DCM) solution upon reaction with dioxygen and thus is in good agreement. Dioxygen reactivity of **1** may be seen in this regard as the dioxygen reactivity of a diiron(II) compound that does not have a O_2X bridging unit.

Reactivity of 5 with Superoxide and Dioxygen. Compound **5** reacts rapidly with superoxide to form an unstable green species, presumably a peroxo complex that decomposes within 1 h at RT to form a light-brown/yellow solution (Figure 1c). Compound **5** did not show any reactivity toward TEMPO. On the other hand, **5** reacted with dioxygen at RT (Figure 1d) to form a dark-green diiron(III,III) peroxo compound featuring an absorption maximum at 595 nm (ε = 2960 ± 210 M^{-1} cm^{-1}) resembling the spectroscopic signature obtained by treatment of **1** with dioxygen. The green solution slowly decays with full bleaching of the band at 595 nm within 1 day at RT (Figure 1f) and a color change to light brown. Appearance of a visible band at 588 nm was also reported upon exposure of a DCM solution of **3**[34] to dioxygen at −60 °C. Compound **5** presumably generates a transient diiron(III) superoxo species, which, in turn, reacts with **5** to yield a metastable diiron(III) peroxo compound (green, λ_{max} = 595 nm) and another diiron(III) compound. This sequence has been studied by RR spectroscopy, Mössbauer spectroscopy, EPR spectroscopy, and electrochemistry, and the results are discussed in the corresponding sections below. The formation of the dark-green solution upon reaction of **5** with dioxygen could be partially reversed upon bubbling nitrogen through it for 15 min. Bubbling dioxygen for 2 min into this brown solution again generated the green species. Prolonged incubation times did not increase the absorbance of the 595 nm band. Also, the more time spent, the more incapable the solution was of showing dioxygen reactivity owing to slow

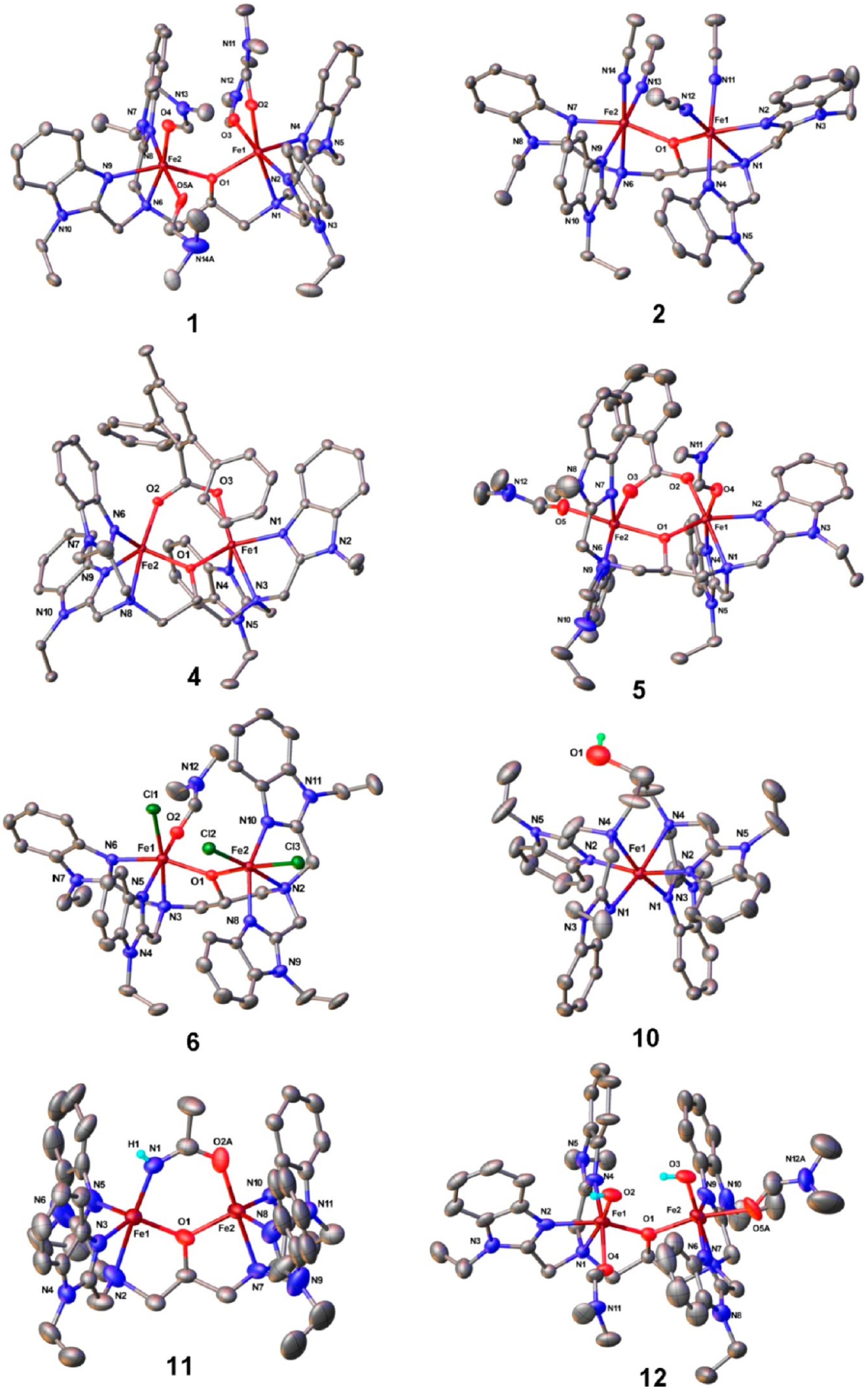

Figure 2. Molecular structures of selected compounds with 50% probability thermal ellipsoids and partial atom-labeling schemes. Hydrogen atoms are omitted for clarity with a few exceptions.

decomposition of the green solution, as shown in Figure 1e. Unlike **5**, **1** forms a highly unstable peroxo species that decomposes rapidly at RT (Figure 1a) compared with decomposition of **5** + O_2 (Figure 1e). Complete reversibility was not observed, as seen by the slow decrease in the absorbance of the regenerated green species in Figure 1f. This

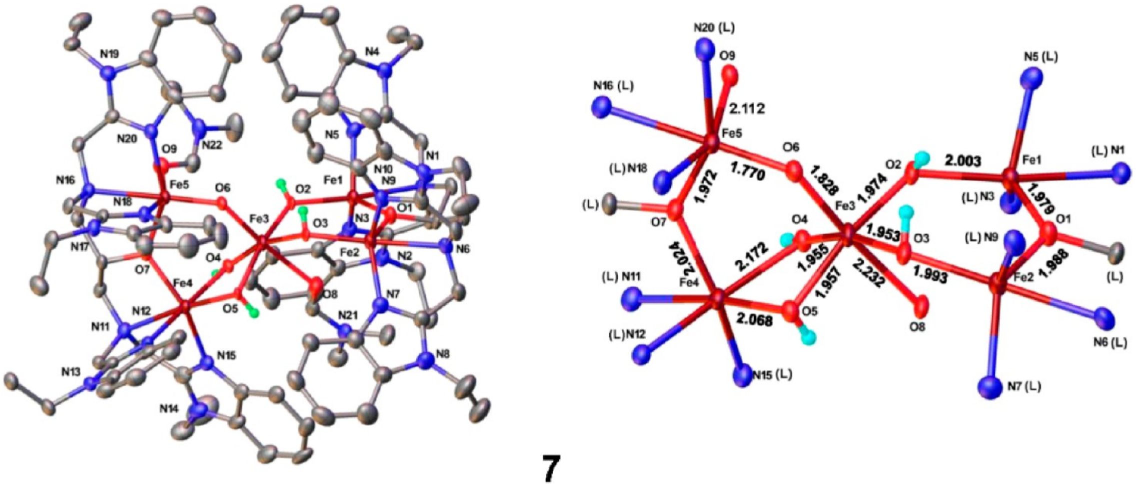

7

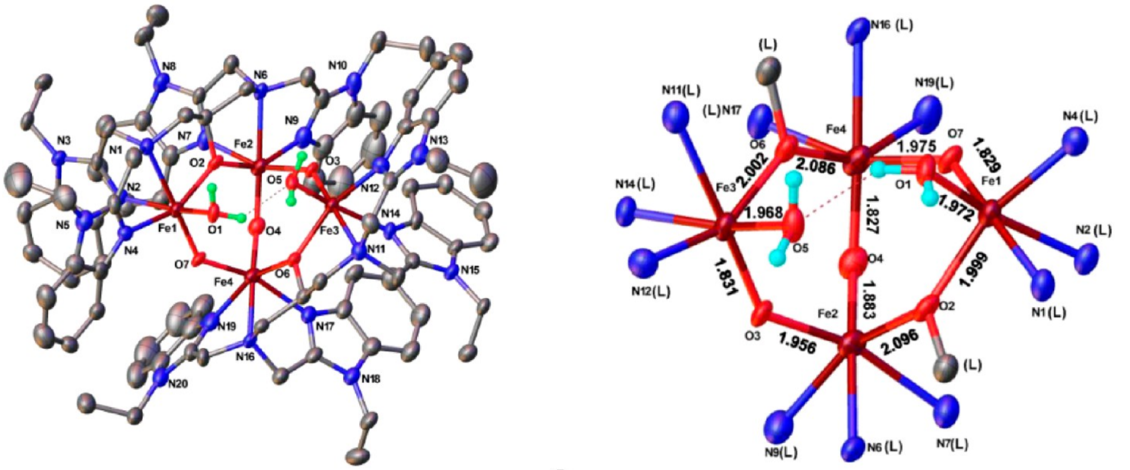

8

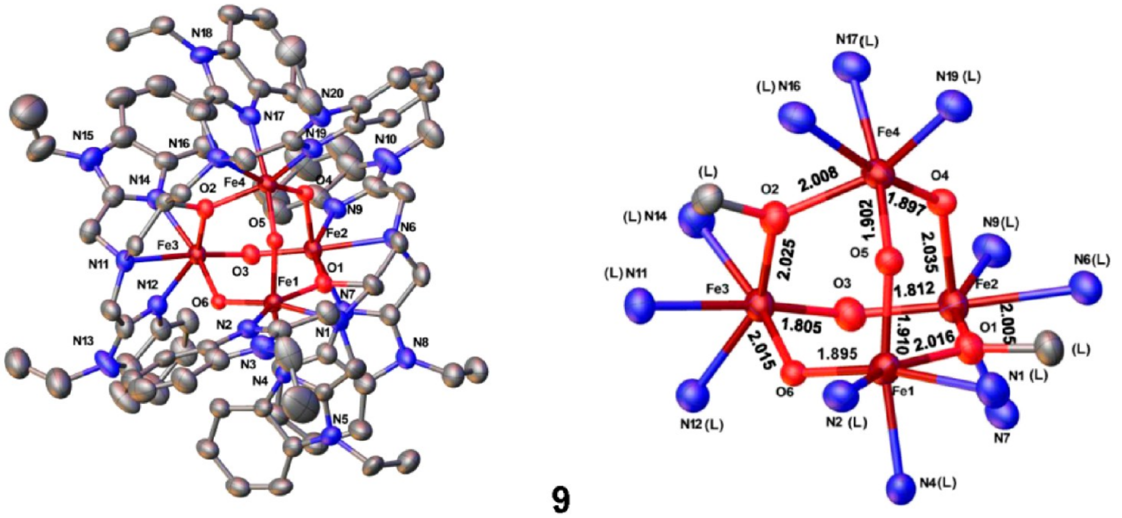

9

Figure 3. Molecular structures of selected compounds shown with 50% probability thermal ellipsoids and partial atom-labeling schemes. Also shown are the core structures with bond distances. Hydrogen atoms are omitted for clarity with some exceptions.

result is in agreement with its observed instability in solution, shown in Figure 1e. Attempts to isolate the light-brown species yielded very tiny brown crystals that were insufficient for single-crystal X-ray structure analysis.

X-ray Structures. Molecular structures of **1**−**12** (except **3**[34]) are presented in Figures 2 and 3. Selected bond distances and angles are provided in Tables S1 and S2, respectively, in the Supporting Information. Compounds **1**, **2**, and **12** have very similar structures, with either DMF (**1** and **12**) or MeCN (**2**) as coordinating solvents. Compounds **3**,[34] **4**, **5**, and **11** have similar structures, differing only in the nature of the bidentate bridging ligand, which is either benzoate (**3** and **5**), 2,6-diphenyl-4-methylbenzoate (**4**), or acetamide (**11**). In contrast to its acetonitrile analogue reported recently,[31] the crystallographic unit cell of **5** contains two independent molecules having different Fe−O bond distances. This situation occurs in X-ray structures of three different crystals from three different batches of **5**. The two benzimidazoles are cis to each other on iron(III) and trans to each other on iron(II). The opposite situation was found in the case of the acetonitrile analogue.[31] Compound **5** has been identified as a class II mixed-valent $Fe^{II}Fe^{III}$ species, based on X-ray structural, electrochemical, EPR, and Mössbauer spectroscopic analyses. Compound **5** displays two different $Fe-O_{carboxylate}$ distances [1.947(2), 2.069(2) Å and 1.961(2), 2.050(3) Å] and two different $Fe-O_{ligand}$ distances [1.929(2), 2.047(2) Å and 1.947(2), 2.035(2) Å] that also differ in the two crystallographically independent molecules. These results are consistent with the different sets of Fe−O bond distances observed in previously reported class II mixed-valent compounds.[25,26]

The core structures of cluster compounds **7**−**9** along with Fe−O bond distances are shown in Figure 3. Compound **7** is a mixed oxo−hydroxo-bridged cluster and contains a $2Fe^{III}/3Fe^{II}$ configuration based on X-ray structural analysis. The differential protonation of the bridging ligands is manifest by the two shorter Fe−μ-O distances of 1.770(4) and 1.829(4) Å and eight longer Fe−μ-OH distances ranging from 1.953(4) to 2.171(4) Å. Compound **8** is an oxo-bridged Fe_4 cluster containing two iron(II) and two iron(III) centers. This compound also displays four short $Fe^{III}-O_{bridging}$ distances, ranging from 1.828(3) to 1.831(3) Å, and two longer distances of 1.955(3) Å, whereas the $Fe-O_{ligand}$ distances are almost invariant (Figure 3). Compound **9** is also an oxo-bridged Fe_4 cluster that adopts an all-ferric adamantane core structure with a broad range of Fe−μ-O distances [1.805(3)−2.035(3) Å]. Two sets of iron(III) sites occur, with Fe−μ-O distances in the ranges 1.805−1.812 and 2.015−2.035 Å in one set and 1.902−1.910 and 1.895−1.897 Å in the other set.

Mössbauer Spectroscopy. Compounds **1**, **2**, **4**−**6**, and **9** and reactive species generated upon reaction of **1** and **5** with dioxygen were examined by ^{57}Fe Mössbauer spectroscopy at 77 K. The Mössbauer spectra are shown in Figures 4 and 5, and the parameters are provided in Table 3. As expected, diiron(II) compounds **1** and **2** exhibit almost identical isomer shifts and quadrupole splittings. These parameters are also very similar to those of **4** (Table 3). Mössbauer data for all three of these compounds correspond to high-spin iron(II). The diiron(III) compound **6** displays two-site spectra in a 1:1 ratio with identical isomer shifts but distinctly different quadrupole splitting values (Table 3) as a result of the different coordination environments of the two iron sites (Figure 2). Compound **9** gives rise to two quadrupole doublets with very similar isomer shifts but different quadrupole splitting values (Table 3) owing to the presence of two sets of iron(III) sites.

Table 3. Mössbauer Parameters at 77 K for Selected Compounds and Reactive Intermediates

compound	δ (mm s^{-1})	ΔE_Q (mm s^{-1})	area (%)
1	1.19	2.99	100
2	1.17	2.92	100
4	1.06	2.99	100
5	1.17	3.25	50
	0.48	0.71	50
6	0.46	0.37	50
	0.47	1.17	50
9	0.51	1.82	50
	0.45	0.99	50
1[a]	1.21	2.94	100
1 + O_2[a]	1.19	3.02	54
	0.46	0.97	46
5 + O_2, 25 min[a]	1.22	3.24	32
	0.52	0.53	32
	0.40	0.82	18
	0.57	0.91	18
5 + O_2, 24 h[a]	0.44	0.76	70
	0.49	1.59	30

[a] Samples loaded in frozen DMF.

Mössbauer spectra of **5** at 77 K exhibit two well-resolved doublets (Figure 4) in a 1:1 ratio with δ = 0.48 mm s^{-1}, ΔE_Q = 0.71 mm s^{-1} and δ = 1.17 mm s^{-1}, ΔE_Q = 3.25 mm s^{-1}, respectively, consistent with a high-spin iron(II)−iron(III) formulation.[51] This observation is in accordance with parameters observed in the case of its acetonitrile analogue $[Fe_2(N\text{-Et-HPTB})(\mu\text{-PhCOO})(MeCN)_2](ClO_4)_3$[31] (120 K, δ = 0.46 mm s^{-1}, ΔE_Q = 0.52 mm s^{-1}; δ = 1.11 mm s^{-1}, ΔE_Q = 3.06 mm s^{-1}) and other mixed-valent compounds such as $[Fe^{II}Fe^{III}BPMP(OPr)_2(BPh_4)_2$,[25] $[Na][Me_4N][Fe_2(HXTA)(OAc)_2]$,[29] $[Fe^{II}Fe^{III}L\text{-py}(CH_3COO)_2](BF_4)_2$,[28] and $[Fe^{II}Fe^{III}L\text{-py}(PhCOO)_2](BF_4)_2$.[28] The observation of discrete quadrupole doublets for **5** at 77 K as well as at RT (Figure S2 in the Supporting Information) indicates that intervalence electron transfer is slow on the Mössbauer time scale (10^7 s^{-1}) at 77 K, similar to the reported case of $[Fe^{II}Fe^{III}(BPMP)(OPr)_2](BPh_4)_2$.[25] Measurements at RT, however, show coalescence of the doublets to a small extent (δ = 0.32 mm s^{-1}, ΔE_Q = 0.71 mm s^{-1}; δ = 1.12 mm s^{-1}, ΔE_Q = 2.56 mm s^{-1}), suggesting the onset of intermediate electron exchange in **5**. The observed decrease in the isomer shift is also in agreement with the fact that, owing to the second-order Doppler effect, Mössbauer isomer shifts diminish by approximately 0.0006 mm s^{-1} for each 1 K increase in temperature.[52] Similar coalescence effects were observed with $Na(Me_4N)[Fe_2(HXTA)(OAc)_2]$,[26] whereas emergence of a valence-detrapped doublet in addition to valence-trapped doublets at RT occurs in the case of $[Fe^{II}Fe^{III}(bimp)(\mu\text{-}O_2CCH_3)_2](ClO_4)_2$.[27] Reaction of **5** with dioxygen was examined by Mössbauer spectroscopy (Figure 5). Formation of a green solution upon bubbling dioxygen into a DMF solution of **5** was monitored by UV−vis spectroscopy (development of λ_{max} = 595 nm absorbance); after 25 min (as shown in Figure 1d,) the solution was frozen at 77 K, and Mössbauer data were collected. The parameters and nature of the fitting suggested that the green solution contains a mixture of unreacted **5**, a diiron(III) peroxo species, and another high-spin iron(III) species. This result can be explained by initial formation of a diiron(III) superoxo species that immediately reacts with the remaining **5** to form a diiron(III) peroxo species (δ = 0.57 mm s^{-1}) and another diiron(III) species (δ = 0.40 mm s^{-1}). Mössbauer parameters displayed by the diiron(III) peroxo species are very similar to those of an X-ray structurally characterized *cis*-1,2-μ-peroxodiiron(III) compound.[53] Data were collected again after the sample was kept at RT for 24 h to characterize the light-brown species. This sample required two site fittings with nearly equal isomer shifts but with different quadrupole splittings, indicating formation of a high-spin iron(III) compound/compounds with different coordination environments for the iron centers.

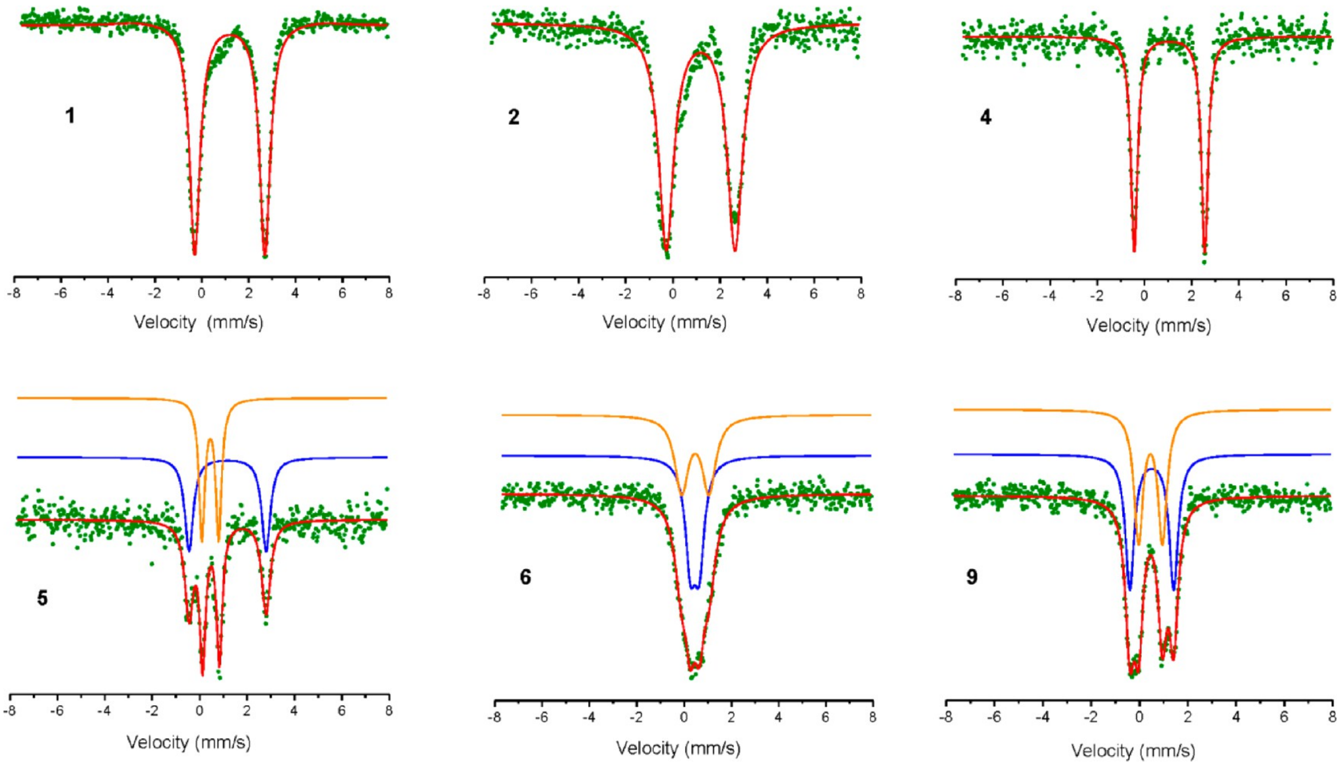

Figure 4. ^{57}Fe Mössbauer spectra of selected compounds as solid samples at 77 K.

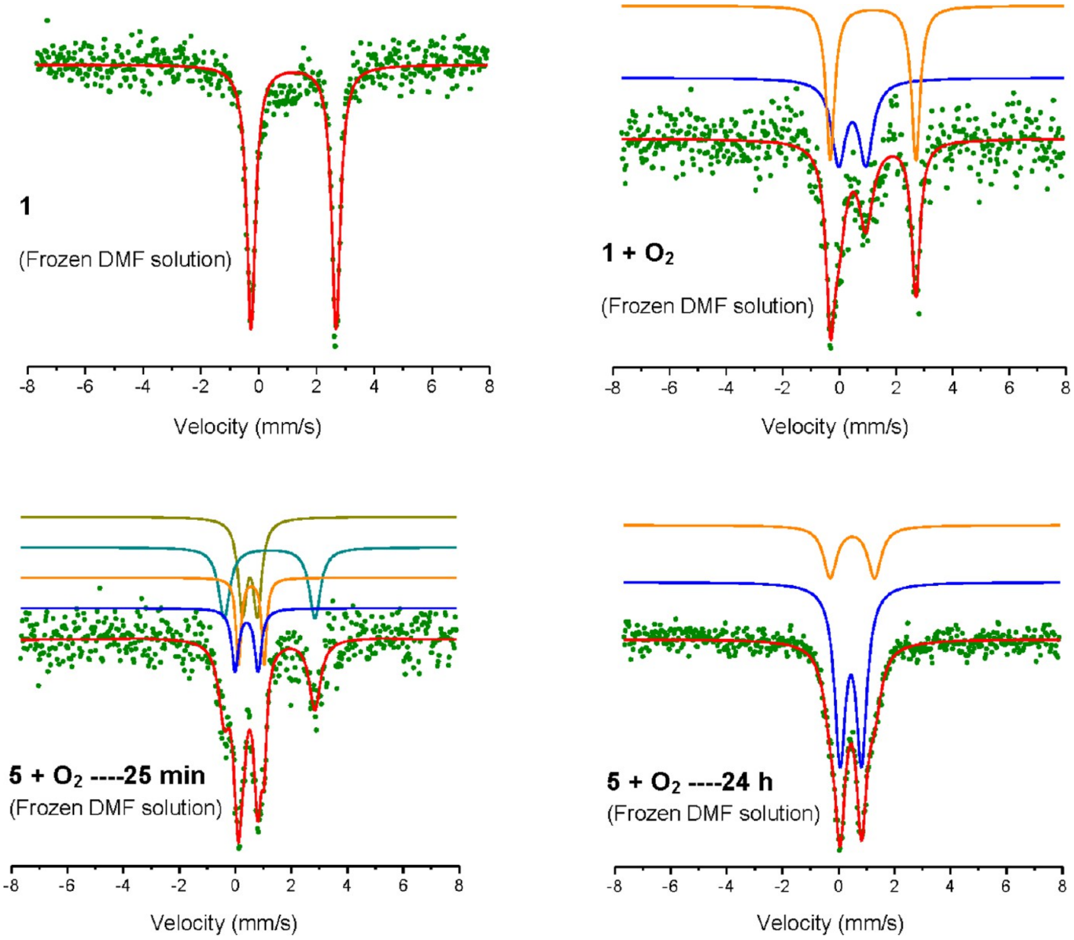

Figure 5. ^{57}Fe Mössbauer spectra of selected compounds and reactive intermediates at 77 K.

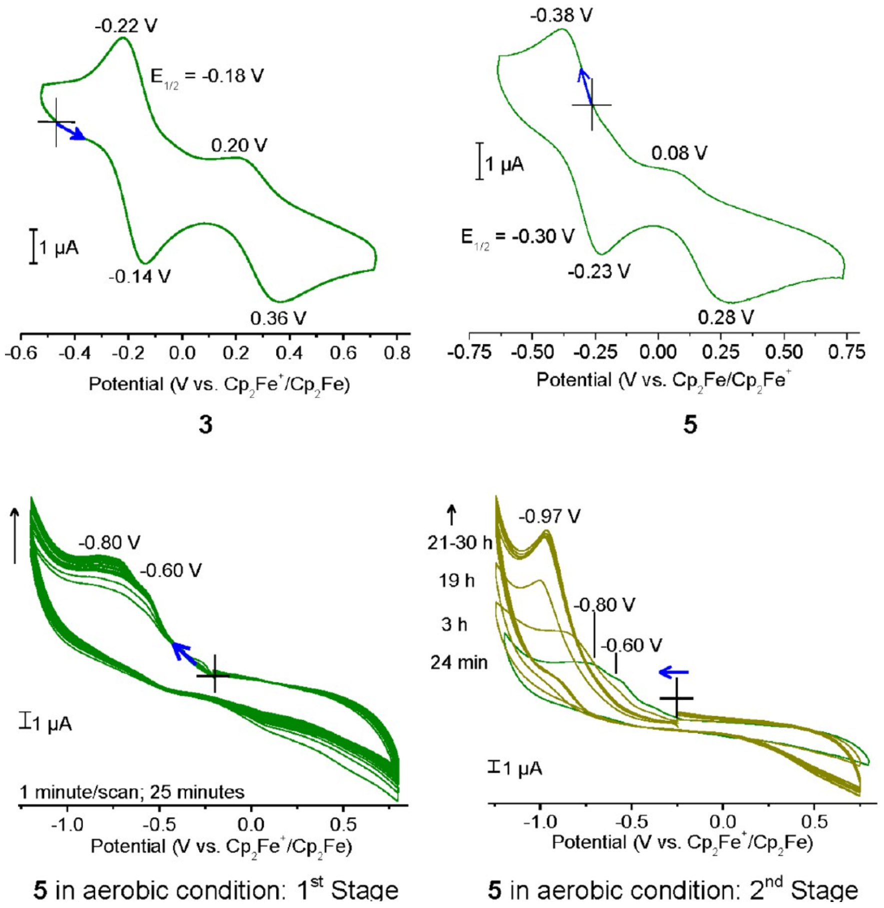

Figure 6. Cyclic voltammetric traces of **3** and **5** (glassy carbon working electrode) in DMF. Also shown is the monitoring of dioxygen reactivity of **5** (platinum working electrode). Scan rate = 100 mV s^{-1}, except in the case of **4** (50 mV s^{-1}).

Formation of a peroxo complex upon reaction of **1** with dioxygen was also examined by Mössbauer spectroscopy (Figure 5). In this experiment, a concentrated DMF solution (70 mg of **1** in 2 mL of DMF) was frozen in liquid nitrogen, and Mössbauer data were collected. The sample was then warmed to 0 °C under nitrogen, and dioxygen gas was bubbled into it for 2 s. The resulting dark-green solution was immediately frozen in liquid nitrogen, and Mössbauer data were measured. The frozen green solution exhibited two quadrupole doublets, with one site having virtually identical isomer shifts and quadrupole splittings as observed for **1**, either as a solid sample or a frozen DMF solution. The other site displayed an isomer shift of 0.46 mm s^{-1} and a quadrupole splitting of 0.97 mm s^{-1}, indicating the formation of a diiron(III) peroxo species. Possible contamination by **8** and **9** can be neglected considering their characteristics, especially the nonquivalent iron sites in **8**, Mössbauer parameters observed for **9**, and much longer time required for formation of **9** even at RT. Mössbauer parameters for an X-ray structurally characterized *cis*-1,2-μ-peroxodiiron(III) compound, $[Fe_2(Ph\text{-}bimp)(C_6H_5COO)(O_2)](BF_4)_2$, are reported as δ = 0.58 mm s^{-1}, ΔE_Q = 0.74 mm s^{-1}; δ = 0.65 mm s^{-1}, ΔE_Q = 1.70 mm s^{-1}, ratio of areas 1.1:1, and are assigned to two distinct high-spin iron(III) centers consistent with different $Fe-O_{pereoxo}$ bond distances observed by X-ray structural characterization.[53] The lower isomer shift in the putative peroxo compound obtained from **1** can be attributed to the increased electron density around the iron(III) centers. This increased electron density is due to the absence of a carboxylate bridge, with its electron-withdrawing properties, and the presence of alkoxide ligation and an ethyl-substituted imidazole-based ligand, both electron-donating, instead of phenoxide ligation and a phenyl-substituted imidazole-based ligand, both less electron-donating. Similar arguments may be invoked to explain the differences in isomer shift (0.66 mm s^{-1}) and quadrupole splitting (1.40 mm s^{-1}) from those reported for $[Fe_2(\mu\text{-}1,2\text{-}O_2)(\mu\text{-}O_2CCH_2Ph)_2\{HB(pz')_3\}_2]$.[54] Also, X-ray structural characterization of the peroxo compound generated by reaction of **3** with dioxygen in the presence of triphenylphosphine oxide (Ph_3PO) in MeCN revealed the formulation $[Fe_2(O_2)(N\text{-}Et\text{-}HPTB)(Ph_3PO)_2](BF_4)_3$.[35] Contrary to expectations, the benzoate bridge was absent in the crystalline dioxygen adduct. This result also suggests that **1** may form an analogous peroxo compound, which might have the formula $[Fe_2(O_2)(N\text{-}Et\text{-}HPTB)(DMF)_2](BF_4)_3$.

Electrochemistry. Cyclic voltammetric traces for compounds **3** and **5**, obtained using a glassy carbon working electrode, are shown in Figure 6. Compound **3** exhibited a reversible oxidation at $E_{1/2}$ = −0.18 V (ΔE = 80 mV, i_{pa}/i_{pc} = 1.1; $E_{1/2}$ = −0.31 V, ΔE = 60 mV, i_{pa}/i_{pc} = 1.1 with a platinum working electrode) along with a quasi-reversible oxidation at 0.36 V (0.17 V with a platinum working electrode). The redox processes involved during cyclic voltammetry of **3** can most likely be presented as follows:

$$Fe^{II}Fe^{II} \underset{+e}{\overset{-e}{\rightleftharpoons}} Fe^{II}Fe^{III} \underset{+e}{\overset{-e}{\rightleftharpoons}} Fe^{III}Fe^{III} \longrightarrow \text{Unknown species}$$

Scheme 2. Schematic Depiction of the Reaction of 5 with Dioxygen

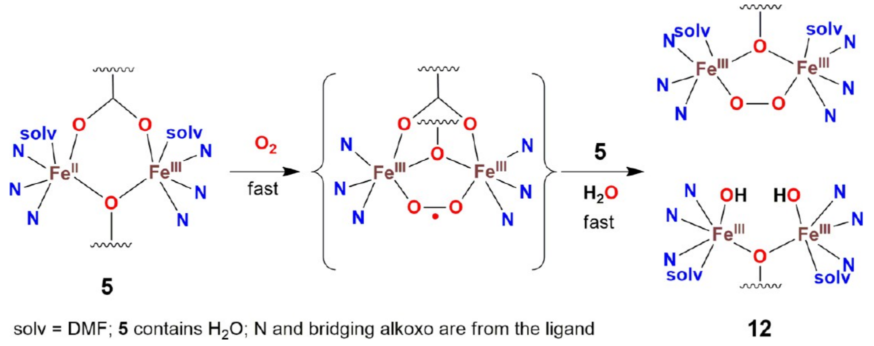

solv = DMF; **5** contains H_2O; N and bridging alkoxo are from the ligand

These two well-separated redox processes explain the generation of a stable mixed-valent species. The assignment of electrochemical reduction and oxidation events of compound **3** is further supported by electrochemical investigations of **5**. The mixed-valent $Fe^{II}Fe^{III}$ compound **5** shows a quasi-reversible reduction at $E_{1/2}$ = −0.30 V with ΔE = 150 mV and i_{pc}/i_{pa} = 1.2 ($E_{1/2}$ = −0.29 V, ΔE = 100 mV, and i_{pa}/i_{pc} = 1.1 with a platinum working electrode). Additionally, an irreversible oxidation event occurred at 0.28 V (0.18 V with a platinum working electrode). The similarity of both cyclic voltammograms thus further supports the presence of a $Fe^{II}Fe^{III}$ species in the case of compound **5** and generation of the same species during one-electron oxidation of **3**. In addition, the cyclic voltammograms highlight the potential of both compounds to adopt $Fe^{II}Fe^{II}$, mixed-valent $Fe^{II}Fe^{III}$, and $Fe^{III}Fe^{III}$ states. For both compounds, the oxidation of $Fe^{II}Fe^{III}$ species generates an unstable $Fe^{III}Fe^{III}$ species, which could not be isolated and was visible as an irreversible reduction of the $Fe^{III}Fe^{III}$ species in the cyclic voltammetric experiments.

The dioxygen reactivity of **5** was also examined by electrochemistry in a DMF solution of **5** through which dioxygen was bubbled (Scheme 2). The cyclic voltammograms using a platinum working electrode appear in Figure 6. Facile generation of at least two irreversible reduction peaks occurred within 25 min at −0.60 and −0.80 V, respectively. Within 24 h, these two peaks gradually vanish and a new reduction peak at −0.97 V is generated. These findings can be rationalized by assuming the formation of an unstable diiron(III) species within 25 min that is converted to a more stable diiron(III) complex with time.

EPR Spectroscopy. Mixed-valent diiron(II,III) compounds encountered in small molecules[24,26−28,30,31] and in biological samples[55] are often successfully characterized by EPR spectroscopy. Most mixed-valent diiron(II,III) compounds in a low-symmetry ligand field exhibit signals with $\langle g_{av} \rangle$ less than 2, characteristic of an $S = {}^1/_2$ system that results from antiferromagnetic coupling of a high-spin iron(III) ion ($S = {}^5/_2$, ^{6}A state) with a high-spin iron(II) ion (S = 2, ^{5}T state from splitting of ^{5}D state) under the weak field approximation.[55] Compound **5** in a frozen 1:1 DMF/MeCN solution displayed a $g < 2$ EPR signal (Figure S3 in the Supporting Information) at 4 K. A similar $g < 2$ EPR spectrum was obtained when a solution of **5** in MeCN was recorded (Figure 7). The coordinated DMF molecules in **5** are fully or at least partially replaced by MeCN in this case, thereby generating a MeCN-coordinated analogue of **5**. This reasoning is further supported by the report of a very similar EPR spectrum for $[Fe_2(N\text{-}Et\text{-}HPTB)(\mu\text{-}PhCOO)(MeCN)_2](ClO_4)_3$.[31]

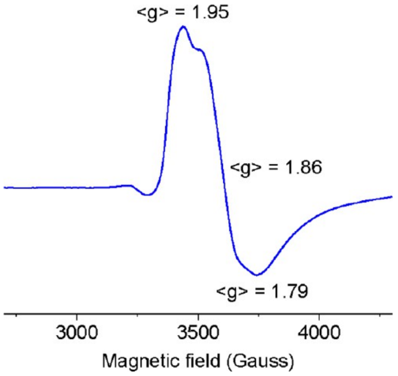

Figure 7. EPR spectra of **5** in MeCN at 4 K. Conditions: [**5**] = 0.2 mM, 9.39 GHz microwave frequency, 20 mW microwave power, 10 G modulation amplitude, and 0.2 s time constant.

RR Spectroscopy. RR spectra of the green species generated upon reaction of **5** with dioxygen were obtained at 110 K with 647 nm excitation. Fe−O stretching vibrations were observed at 466/476 and 456 cm^{-1} for samples prepared with $^{16}O_2$ and $^{18}O_2$, respectively (Figure 8). The corresponding O−O stretches for the diiron(III) peroxo complex occur near 895 cm^{-1} for $^{16}O_2$ and can be observed near 845 cm^{-1} for $^{18}O_2$ despite its overlap with a strong DMF solvent vibration (Figure 8). These vibrational frequencies match our previous characterization of peroxo complexes using the same ligand platform.[56] There is no $^{16/18}$O-sensitive mode in the 1050−1250 cm^{-1} region where ν(O−O) of iron(III) superoxo species are expected. The RR data thus support the assignment of the green species as a diiron(III) peroxo complex formed by intermolecular electron transfer.

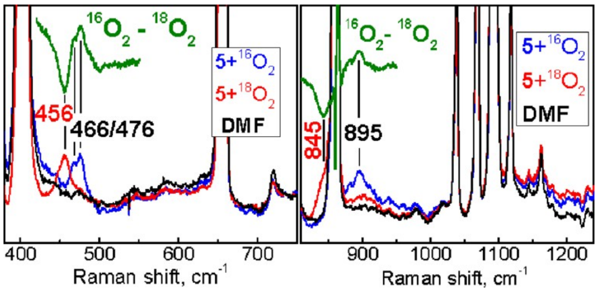

Figure 8. RR spectra of an oxygenated DMF solution of **5** at 110 K with a 647 nm excitation.

*Concluding Remarks for Reaction of **5** with Dioxygen.* From the electronic absorption, RR, and Mössbauer spectroscopic results, together with electrochemistry, it can be concluded that **5** reacts very rapidly with oxygen to form a diiron(III) superoxo complex. This putative superoxo species immediately reacts with **5** present in solution to form the green diiron(III) peroxo compound and a diiron(III) complex that could be **12**, or at least similar to **12**, because **12** was isolated by "water-assisted" oxidation of **5**. A notable feature of **12** is that the bridging carboxylate is lost. Loss of carboxylates upon formation of diiron(III) peroxo compounds in the H*N*-Et-HPTB ligand platform has precedence,[35] the reasons for which have been recently explained.[38] This assumption is supported by the appearance of a high-spin iron(III) site at $\delta = 0.40$ mm s^{-1}, as discussed for the reaction of **5** with dioxygen (Figure 4) in the Mössbauer section. With time, the diiron(III) peroxo compound changes or combines with itself or with the other diiron(III) species to yield more stable di- or polynuclear iron(III) compound/compounds similar to **8** or **9**. A reasonable description for the decomposition of related peroxo compounds to form polyiron(III) compounds can be found elsewhere.[37]

SUMMARY

A new diiron(II) system, $[Fe_2(N\text{-Et-HPTB})(DMF)_4](BF_4)_3$ (**1**), has been developed that can be used as a starting material for the synthesis of carboxylate-bridged diiron complexes. Addition of dioxygen to **1** leads to the formation of a highly unstable peroxo species, and its fast decomposition to polyiron complexes is described. Controlled one-electron oxidation of **1** (or **3**) generates the mixed-valent diiron(II,III) compound **5**, which has been isolated and characterized. Compound **5** features a diiron core doubly bridged by a carboxylate and a ligand-derived alkoxo group. Such a compound can be considered a reasonable model for diiron(II,III) centers in dioxygen-activating enzymes such as MIOX. Reversible dioxygen reactivity of this diiron(II,III) species (**5**), leading to the formation of a diiron(III) peroxo compound, is described for the first time. The description of such fascinating reactivity in this report should stimulate further investigation using related diiron(II,III) compounds in different ligand environments.

ASSOCIATED CONTENT

Ⓢ Supporting Information

X-ray crystallographic data for compounds **1**−**12** in CIF format, selected bond lengths and angles, RT Mössbauer spectroscopic data of **5**, EPR spectra of **5** in DMF/MeCN (1:1), electronic absorption spectroscopic signatures of selected compounds, and monitoring for the reaction of **5** with dioxygen. This material is available free of charge via the Internet at http://pubs.acs.org.

AUTHOR INFORMATION

Corresponding Authors

*E-mail: moennelo@ohsu.edu.
*E-mail: lippard@mit.edu.

Notes

The authors declare no competing financial interest.

ACKNOWLEDGMENTS

This work was supported by Grant GM 032134 (S.J.L.) and GM 074785 (P.M.L.) from the National Institute of General Medical Sciences. U.-P.A. thanks the Alexander-von-Humboldt Foundation for a postdoctoral fellowship. The authors acknowledge A. D. Liang for her help in collecting EPR data.

REFERENCES

(1) Merkx, M.; Kopp, D. A.; Sazinsky, M. H.; Blazyk, J. L.; Muller, J.; Lippard, S. J. *Angew. Chem., Int. Ed.* **2001**, *40*, 2782−2807.
(2) Feig, A. L.; Lippard, S. J. *Chem. Rev.* **1994**, *94*, 759−805.
(3) Lippard, S. J. *Philos. Trans. R. Soc., A* **2005**, *363*, 861−877.
(4) Wallar, B. J.; Lipscomb, J. D. *Chem. Rev.* **1996**, *96*, 2625−2657.
(5) Rosenzweig, A. C.; Nordlund, P.; Takahara, P. M.; Frederick, C. A.; Lippard, S. J. *Chem. Biol.* **1995**, *2*, 409−418.
(6) Rosenzweig, A. C.; Frederick, C. A.; Lippard, S. J.; Nordlund, P. *Nature* **1993**, *366*, 537−543.
(7) Rosenzweig, A. C.; Lippard, S. J. *Acc. Chem. Res.* **1994**, *27*, 229−236.
(8) Tinberg, C. E.; Lippard, S. J. *Acc. Chem. Res.* **2011**, *44*, 280−288.
(9) Tshuva, E. Y.; Lippard, S. J. *Chem. Rev.* **2004**, *104*, 987−1011.
(10) Do, L. H.; Lippard, S. J. *J. Inorg. Biochem.* **2011**, *105*, 1774−1785.
(11) Friedle, S.; Reisner, E.; Lippard, S. J. *Chem. Soc. Rev.* **2010**, *39*, 2768−2779.
(12) Tolman, W. B.; Que, J. L. *J. Chem. Soc., Dalton Trans.* **2002**, 653−660.
(13) Que, J. L. *J. Chem. Soc., Dalton Trans.* **1997**, 3933−3940.
(14) Que, L.; Dong, Y. *Acc. Chem. Res.* **1996**, *29*, 190−196.
(15) Sugimoto, H.; Nagayama, T.; Maruyama, S.; Fujinami, S.; Yasuda, Y.; Suzuki, M.; Uehara, A. *Bull. Chem. Soc. Jpn.* **1998**, *71*, 2267−2279.
(16) Suzuki, M. *Pure Appl. Chem.* **1998**, *70*, 955−960.
(17) Edmondson, D. E.; Huynh, B. H. *Inorg. Chim. Acta* **1996**, *252*, 399−404.
(18) Kurtz, D. M. *J. Biol. Inorg. Chem.* **1997**, *2*, 159−167.
(19) Brown, P. M.; Caradoc-Davies, T. T.; Dickson, J. M. J.; Cooper, G. J. S.; Loomes, K. M.; Baker, E. N. *Proc. Natl. Acad. Sci. U.S.A.* **2006**, *103*, 15032−15037.
(20) Bollinger, J. M.; Diao, Y.; Matthews, M. L.; Xing, G.; Krebs, C. *Dalton Trans.* **2009**, 905−914.
(21) Charalampous, F. C. *J. Biol. Chem.* **1959**, *234*, 220−227.
(22) Charalampous, F. C.; Lyras, C. *J. Biol. Chem.* **1957**, *228*, 1−13.
(23) Moskala, R.; Reddy, C. C.; Minard, R. D.; Hamilton, G. A. *Biochem. Biophys. Res. Commun.* **1981**, *99*, 107−113.
(24) Hartman, J. A. R.; Rardin, R. L.; Chaudhuri, P.; Pohl, K.; Wieghardt, K.; Nuber, B.; Weiss, J.; Papaefthymiou, G. C.; Frankel, R. B.; Lippard, S. J. *J. Am. Chem. Soc.* **1987**, *109*, 7387−7396.
(25) Borovik, A. S.; Que, L., Jr. *J. Am. Chem. Soc.* **1988**, *110*, 2345−2347.
(26) Borovik, A. S.; Papaefthymiou, V.; Taylor, L. F.; Anderson, O. P.; Que, L., Jr. *J. Am. Chem. Soc.* **1989**, *111*, 6183−6195.
(27) Mashuta, M. S.; Webb, R. J.; Oberhausen, K. J.; Richardson, J. F.; Buchanan, R. M.; Hendrickson, D. N. *J. Am. Chem. Soc.* **1989**, *111*, 2745−2746.
(28) Suzuki, M.; Uehara, A.; Oshio, H.; Endo, K.; Yanaga, M.; Kida, S.; Saito, K. *Bull. Chem. Soc. Jpn.* **1987**, *60*, 3547−3555.
(29) Borovik, A. S.; Murch, B. P.; Que, L., Jr.; Papaefthymiou, V.; Munck, E. *J. Am. Chem. Soc.* **1987**, *109*, 7190−7191.
(30) Payne, S. C.; Hagen, K. S. *J. Am. Chem. Soc.* **2000**, *122*, 6399−6410.
(31) Li, F.; Chakrabarti, M.; Dong, Y.; Kauffmann, K.; Bominaar, E. L.; Münck, E.; Que, L., Jr. *Inorg. Chem.* **2012**, *51*, 2917−2929.
(32) Do, L. H.; Lippard, S. J. *J. Am. Chem. Soc.* **2011**, *133*, 10568−10581.
(33) McKee, V.; Zvagulis, M.; Dagdigian, J. V.; Patch, M. G.; Reed, C. A. *J. Am. Chem. Soc.* **1984**, *106*, 4765−4772.
(34) Dong, Y.; Menage, S.; Brennan, B. A.; Elgren, T. E.; Jang, H. G.; Pearce, L. L.; Que, L., Jr. *J. Am. Chem. Soc.* **1993**, *115*, 1851−1859.
(35) Dong, Y.; Yan, S.; Young, V. G.; Que, L., Jr. *Angew. Chem., Int. Ed.* **1996**, *35*, 618−620.
(36) Feig, A. L.; Lippard, S. J. *J. Am. Chem. Soc.* **1994**, *116*, 8410−8411.

(37) Feig, A. L.; Becker, M.; Schindler, S.; van Eldik, R.; Lippard, S. J. *Inorg. Chem.* **1996**, *35*, 2590−2601.

(38) Frisch, J. R.; McDonnell, R.; Rybak-Akimova, E. V.; Que, L., Jr. *Inorg. Chem.* **2013**, *52*, 2627−2636.

(39) Avenier, F.; Herrero, C.; Leibl, W.; Desbois, A.; Guillot, R.; Mahy, J.-P.; Aukauloo, A. *Angew. Chem., Int. Ed.* **2013**, *52*, 3634−3637.

(40) Robin, M. B.; Day, P. In *Advances in Inorganic Chemistry and Radiochemistry*; Emeléus, H. J., Sharpe, A. G., Eds.; Academic Press: New York, 1968; Vol. *10*, pp 247−422.

(41) *APEX II*; Bruker Analytical X-ray Systems Inc.: Madison, WI, 2009.

(42) Spek, A. L. *J. Appl. Crystallogr.* **2003**, *36*, 7−13.

(43) Spek, A. L. *Acta Crystallogr., Sect. D* **2009**, *65*, 148−155.

(44) Sheldrick, G. M. *Acta Crystallogr., Sect. A* **2008**, *64*, 112−122.

(45) Dolomanov, O. V.; Bourhis, L. J.; Gildea, R. J.; Howard, J. A. K.; Puschmann, H. *J. Appl. Crystallogr.* **2009**, *42*, 339−341.

(46) Farrugia, L. J. *J. Appl. Crystallogr.* **1997**, *30*, 565.

(47) Farrugia, L. J. *J. Appl. Crystallogr.* **2012**, *45*, 849−854.

(48) Do, L. H.; Xue, G.; Que, L., Jr.; Lippard, S. J. *Inorg. Chem.* **2012**, *51*, 2393−2402.

(49) Connelly, N. G.; Geiger, W. E. *Chem. Rev.* **1996**, *96*, 877−910.

(50) Stiddard, M. H. B.; Townsend, R. E. *J. Chem. Soc. A* **1969**, 2355−2357.

(51) Greenwood, N. N.; Gibb, T. C. *Mössbauer Spectroscopy*; Chapman and Hall: London, 1971; pp 113−168.

(52) Lang, G.; Marshall, W. *Proc. Phys. Soc.* **1966**, *87*, 3−34.

(53) Ookubo, T.; Sugimoto, H.; Nagayama, T.; Masuda, H.; Sato, T.; Tanaka, K.; Maeda, Y.; Okawa, H.; Hayashi, Y.; Uehara, A.; Suzuki, M. *J. Am. Chem. Soc.* **1996**, *118*, 701−702.

(54) Kim, K.; Lippard, S. J. *J. Am. Chem. Soc.* **1996**, *118*, 4914−4915.

(55) Bertrand, P.; Guigliarelli, B.; More, C. *New J. Chem.* **1991**, *15*, 445−454.

(56) Do, L. H.; Hayashi, T.; Moënne-Loccoz, P.; Lippard, S. J. *J. Am. Chem. Soc.* **2010**, *132*, 1273−1275.